JOURNAL OF COATING TECHNOLOGY AND INNOVATION
Jul-Sept 2024, VOL. 2, ISSUE 3, pp. 7-11
https://doi.org/10.61577/jcti.2024.1000012

RESEAPRO JOURNALS

ORIGINAL ARTICLE

OPEN ACCESS

Effect of powder feeding rate on microstructure and properties of Fe-based fine-grained lasers cladding layers

Mingchao Sui[1,2], Hui Zhang[1,2], Wei Zhao[1,2] and Yuexia Lv[1,2]

[1]College of Mechanical Engineering, Qilu University of Technology (Shandong Academy of Sciences), China
[2]Shandong Institute of Mechanical Design and Research, Qilu University of Technology (Shandong Academy of Sciences), China

ABSTRACT

This manuscript investigates the influence of powder feeding rate on the microstructure and properties of vanadium carbide-reinforced fine-grained cladding layers fabricated on nodular cast iron by laser cladding. The results indicate that as the powder feeding rate increases, the crack defects in the cladding layer are significantly improved. All cladding layers are composed of α-Fe and in-situ synthesized vanadium carbide. With the increase in powder feeding rate, the proportion of in-situ synthesized vanadium carbide relatively decreases. The hardness of the cladding layer exhibits a trend of initially increasing and then decreasing with the increase in powder feeding rate. The corrosion resistance of the cladding layer enhances with the increase in powder feeding rate. When the powder feeding rate reaches 6 g/min, the cladding layer demonstrates the best comprehensive performance, including good formation as well as excellent hardness and corrosion resistance.

KEYWORDS

Laser cladding; Nodular cast iron; High wear resistance; Tribocorrosion; Corrosion resistance

ARTICLE HISTORY

Received 16 July 2024;
Revised 19 August 2024;
Accepted 26 August 2024

Introduction

Nodular cast iron is an engineering material with excellent properties. Due to its good wear resistance, castability, as well as good toughness and strength, nodular cast iron is widely used in multiple fields such as the automotive industry, mechanical manufacturing, pipeline systems, and agricultural machinery [1-8]. However, under certain specific working conditions and long-term natural wear and tear, severe wear and corrosion of nodular cast iron are easily induced, causing damage and failure of workpieces, which greatly affects industrial safety and causes industrial economic losses. In order to further expand the application range and service life of nodular cast iron, the research on surface repair and surface modification of nodular cast iron becomes increasingly important [9,10].

At present, in industry, methods such as electron beam welding arc welding, and arc spraying are often used to repair damaged nodular cast iron workpieces. However, since nodular cast iron contains a large amount of spherically distributed graphite, under welding and cladding processes, the graphite particles will melt, resulting in the easy formation of hard and brittle microstructures in the bonding zone and reducing its tensile strength [11-14]. Moreover, during the cooling and shrinking process of welds and cladding layers, relatively high residual stress will be generated, which is extremely likely to cause cracking at the interface [15,16].

Laser cladding is an advanced surface modification technology, which can generate high-performance cladding layers metallurgically bonded to the substrate through high-energy-density laser beams and cladding powders. Commonly used laser cladding powders are three types: iron-based, cobalt-based, and nickel-based [17-23]. Among them, iron-based powders are the most widely used due to their outstanding cost-effectiveness, strong process adaptability, and good bonding with the substrate. The process characteristics of laser cladding enable it to achieve precise local modification without affecting other areas, thereby maximizing material and cost savings. Moreover, compared with other welding processes, the high precision and high controllability of laser cladding can more accurately adjust the heat input, making the forming quality of the cladding layer more controllable [24]. At present, the research on nodular cast iron repair is mostly achieved by optimizing process parameters and cladding powder compositions to adjust the heat input or carbon element content, thereby reducing the generation of hard and brittle structures and cracks. Rui Wang and others used laser cladding technology to control the heat input by adjusting the laser power and fabricated defect-free nickel-based high-corrosion-resistant cladding layers on the surface of nodular cast iron substrates [25]. Runze Wei and others eliminated the defects in the nodular cast iron cladding layer through high-speed laser cladding and greatly enhanced the comprehensive performance of the cladding layer [26]. The research of Pengcong Yang and others revealed the relationship between heat input and crack defects in the iron-based cladding layer of nodular cast iron and prepared defect-free high-performance cladding layers [27]. However, at present, the modification and repair of nodular cast iron by laser cladding are still insufficient. There are few reports on cladding using low-cost powders. The performance of the cladding layer or the cladding process has not reached the optimal state, making it difficult to provide relatively complete guidance and reference opinions for actual production.

In this paper, by changing the powder feeding rate to indirectly adjust the heat input and control the dilution rate, and using the V element to consume the reversely transferred C element in the substrate to reduce hard and brittle structures and achieve the purpose of eliminating crack

*Correspondence: Dr. Hui Zhang, College of Mechanical Engineering, Qilu University of Technology (Shandong Academy of Sciences), Jinan, China, e-mail: zhanghui198787@163.com
© 2024 The Author(s). Published by Reseapro Journals. This is an Open Access article distributed under the terms of the Creative Commons Attribution License (http://creativecommons.org/licenses/by/4.0/), which permits unrestricted use, distribution, and reproduction in any medium, provided the original work is properly cited.

defects. The intention is to prepare a defect-free in-situ synthesized vanadium carbide reinforced Fe-based fine-grained cladding layer on the nodular cast iron substrate, which can provide valuable reference for industrial repair of nodular cast iron.

Experimental

The variable particle size cladding alloy powder is composed of reduced iron powder and ferrovanadium powder (47.80 wt.% V, 0.50 wt.% Al, 2.00 wt.% Si, 0.078 wt.% P, 0.033 wt.% S, 0.480 wt.% C, balance Fe). According to the change of powder feeding rate during the cladding process, the samples are divided into S1-S5. The powder feeding rate and its content ratio are shown in Table 1. The powder is mixed for two hours at a speed of 30 revolutions/min by a V-type powder mixer to make it evenly mixed so that each element can quickly and evenly diffuse in the molten pool during cladding. The substrate is nodular cast iron QT500-14 (3.3-3.6 wt.% C, 1.8-2.2 wt.% Si, 0.3-0.5 wt.% Mn, P≤ 0.1 wt.%, S≤0.15 wt.%, Cu≤0.3 wt.%).

Table 1. Composition ratio and variable parameters of cladding powder.

Sample	FeV50	Fe	Powder Feeding Rate
S1	48.57 wt.%	51.43 wt.%	2 g/min
S2	48.57 wt.%	51.43 wt.%	4 g/min
S3	48.57 wt.%	51.43 wt.%	6 g/min
S4	48.57 wt.%	51.43 wt.%	8 g/min
S5	48.57 wt.%	51.43 wt.%	10 g/min

The cut and polished specimens are subjected to phase analysis using an X-ray diffractometer (Shimadzu XRD-6100). The working voltage, working current, and step speed are set at 40 kV, 30 mA, and 6°/min respectively. The ultra-depth-of-field optical microscopy system (VHX-5000) is used to observe and analyze the microstructure of the cladding layer. The micro-Vickers hardness tester (HXD-1000TMC) is used to measure the hardness of the cross-section of each specimen. The test force is 1.96 N and the holding time is 15 s.

The corrosion test is completed using the Gamary Interface 1000 electrochemical workstation. The corrosion solution is 3.5 wt.% NaCl solution at 293 K. The reference electrode is a saturated calomel electrode, and the working electrode is the treated cladding layer sample. Firstly, an open circuit potential test is carried out, and the time is set to 1800 s. After the open circuit potential is stabilized, the potentiodynamic polarization curve and impedance spectrum test are carried out. The scanning rate of the potential-potentiodynamic polarization curve is 0.5 mV/s. The impedance spectrum test is carried out at the open circuit potential of the sample with an amplitude of 10 mV and a frequency range from 100 kHz to 0.01 Hz.

Results and Discussion

The surface formation and cross-sectional macroscopic morphologies of each cladding layer are shown in Figure 1(a)-(e). The thickness of the S1-S5 cladding layers gradually increases with the increase of powder feeding rate, and the cladding layers are well bonded to the substrate. The surfaces of each cladding layer are continuous and flat, the weld bead distribution is uniform, and the surface formation is good. There are some pores in each cladding layer. It is analyzed that this is because the graphite particles in the substrate melt and react with oxygen in the air to produce some carbon monoxide. During the cladding process, the solidification speed of the molten pool is too fast, and the gas has no time to escape and form pores. A small amount of crack defects are found in the S1 and S2 cladding layers. In the S3-S5 cladding layers, due to the increase of powder feeding rate, the crack defects are significantly reduced. It is speculated that this is because the dilution rate of the nodular cast iron substrate is reduced, reducing the carbon content in the cladding layer and inhibiting the formation of hard and brittle structures.

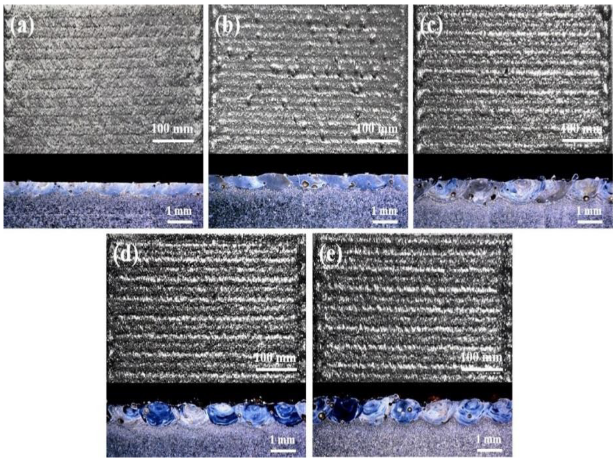

Figure 1. Surface formation and cross-sectional macroscopic morphologies of each cladding layer. (a) S1 cladding layer (b) S2 cladding layer (c) S3 cladding layer (d) S4 cladding layer (e) S5 cladding layer.

Figure 2 shows the X-ray diffraction patterns of each cladding layer. Analysis reveals that each cladding layer is composed of α-Fe and in-situ synthesized V_6C_5. It can be seen that a certain amount of in-situ synthesized vanadium carbide has been successfully generated by relying on the reversely transferred C element in the substrate during the cladding process. By comparing the heights of the main peaks of α-Fe and V_6C_5 in the S1-S5 cladding layers, it is found that the relative content of V_6C_5 gradually decreases with the increase of powder feeding rate. This indicates that the dilution rate of the nodular cast iron substrate is reduced, and the C content in the cladding layer decreases with the increase of powder feeding rate. This explains the alleviation of crack defects in the cladding layer.

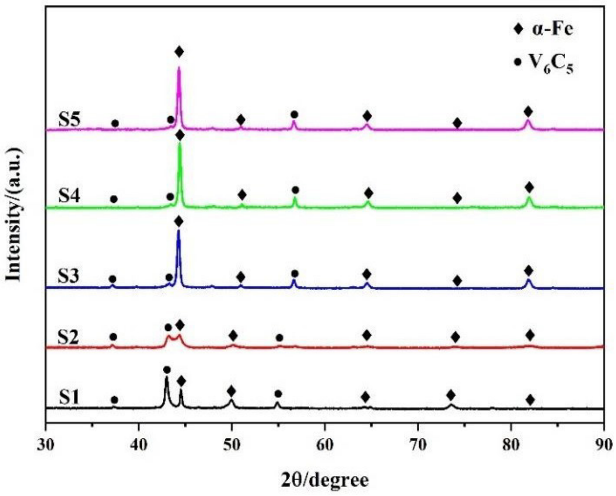

Figure 2. XRD patterns of the cladding layer.

© Reseapro Journals 2024
https://doi.org/10.61577/jcti.2024.1000012

Figure 3(a)-(e) shows the microstructures in the upper-middle part of each cladding layer. As shown in the figure, S1 is mainly composed of dendrites and equiaxed grains, while the S2-S5 cladding layers are mainly composed of a large number of equiaxed grains. There is a large amount of precipitated in-situ synthesized vanadium carbide at the grain boundaries of the S1 cladding layer. However, for the S2-S5 cladding layers, due to the increase in powder feeding rate, the increase in the powder participating in melting reduces the energy acting on the substrate, resulting in a reduction in the dilution rate and a decrease in the C content in the molten pool, leading to a reduction in in-situ synthesized vanadium carbide. The average grain size of the S1-S5 cladding layers (Figure 4) shows a trend of first decreasing and then increasing. With the increase in powder feeding rate, more powder will enter the molten pool during the cladding process. While these powders absorb heat and melt, they will also take away a part of the heat, which will reduce the overall temperature of the molten pool and accelerate the cooling speed of the molten pool, reducing the grain growth time. When the powder feeding rate continues to increase, excessive cladding powder needs to be completely melted, which prolongs the existence time of the molten pool and increases heat accumulation, creating an opportunity for grain growth [28].

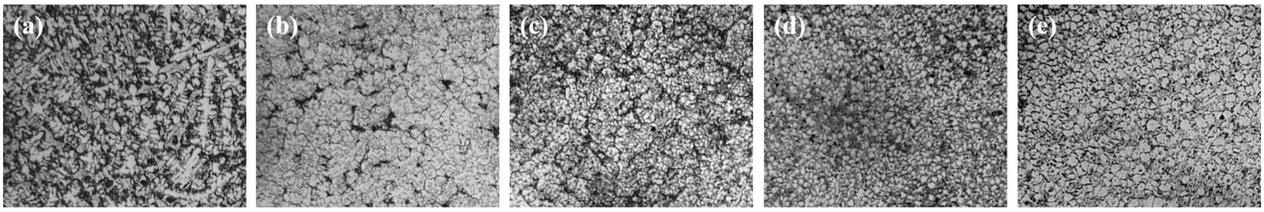

Figure 3. Microstructure morphologies of the cladding layers (a) S1 cladding layer (b) S2 cladding layer (c) S3 cladding layer (d) S4 cladding layer (e) S5 cladding layer.

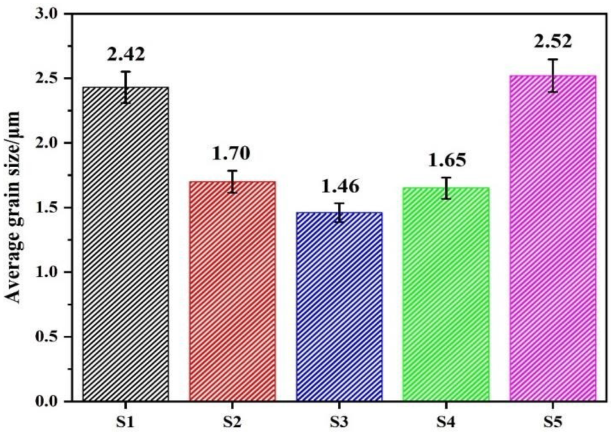

Figure 4. Average grain size of each cladding layer.

The hardness of the S1-S5 cladding layers is shown in Figure 5. The average hardnesses of the S1-S5 cladding layers are 758 $HV_{0.2}$, 835 $HV_{0.2}$, 774 $HV_{0.2}$, 364 $HV_{0.2}$, and 351 $HV_{0.2}$ respectively, showing an overall trend of first increasing and then decreasing. When the powder feeding rate is increased from 2g/min to 4g/min, the dilution rate of the substrate is reduced, and at the same time, the grains become finer, which increases the hardness of the cladding layer. However, as the powder feeding rate continues to increase and the dilution rate is further reduced, the C element reversely transferred from the substrate also decreases correspondingly, resulting in a reduction in the in-situ synthesized vanadium carbide generated in the cladding layer, which causes the hardness of the cladding layer to decrease. The hardness of the S3 cladding layer gradually increases from the surface to the fusion zone. Combined with the change trend of grain size, it indicates that the main reason for this change is that the duration of the molten pool of the S3 cladding layer is too short. While hindering grain growth, it also hinders the uniform diffusion of in-situ synthesized vanadium carbide, resulting in the accumulation of hard phases in the bottom area of the molten pool close to the substrate.

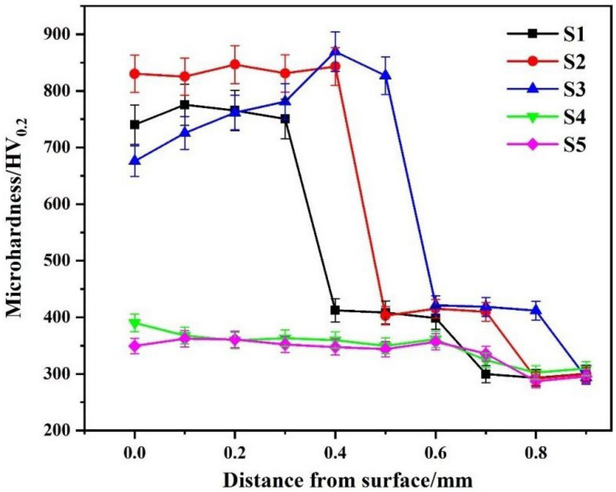

Figure 5. Hardness diagram of each cladding layer.

Figure 6 shows the polarization curve images of the S1-S5 cladding layers. The traditional Taffel method is used to fit the polarization curves, and the fitting results are shown in Table 2. Analyzing the data, it can be found that when the powder feeding rate is gradually increased, the self-corrosion potential of the cladding layer has a positive shift trend, and the self-corrosion current density is significantly reduced.

The more positive the self-corrosion potential is, the weaker the corrosion tendency of the cladding layer. The smaller the self-corrosion current density is, the better the corrosion resistance of the cladding layer. When the powder feeding rate reaches 10g/min, the cladding layer shows the best corrosion resistance. The self-corrosion potential is -0.52242 V, and the self-corrosion current reaches 1.5516 $\mu A/cm^2$, which is only 18.3% of that of the S1 cladding layer. The corrosion resistance is improved by 5.43 times compared to the S1 cladding layer. The reason for the improvement of the corrosion resistance of the cladding layer with the increase of powder feeding rate is mainly due to the reduction of the dilution rate of

© Reseapro Journals 2024
https://doi.org/10.61577/jcti.2024.1000012

the substrate during the increase of powder feeding rate, which makes the content of reversely transferred C element continuously decrease. This leads to a reduction in the generated in-situ synthesized vanadium carbide and alleviates the erosion of the corrosion galvanic cell generated by the substrate and the hard phase. Corrosion mainly occurs preferentially at the grain boundaries. However, for the S1-S3 cladding layers, due to the gradual refinement of grains, the proportion of grain boundaries increases, so the improvement in corrosion resistance is relatively small.

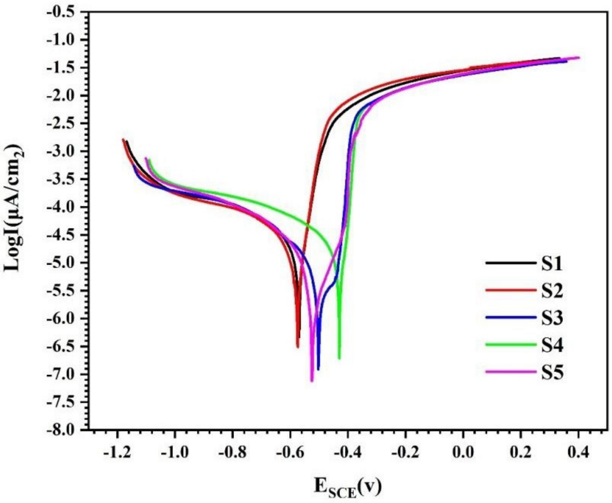

Figure 6. Polarization curves of each cladding layer.

Table 2. Fitting results of polarization curves.

Sample	Ecorr (V)	Icorr (μA/cm2)	Corrosion Rate (mm/year)
S1	-0.56279	8.4267	0.10593
S2	-0.57583	7.9759	0.09271
S3	-0.49541	7.0125	0.08151
S4	-0.50165	2.0497	0.02382
S5	-0.52242	1.5516	0.01359

Conclusions

With the increase of powder feeding rate, the thickness of the cladding layer gradually increases, bonds well with the substrate, has a continuous and flat surface and uniform weld bead distribution. However, there are some pores in each cladding layer. When the powder feeding rate is increased from 2g/min to 4g/min, the dilution rate of the substrate is reduced and the grains are finer, which increases the hardness of the cladding layer. But when the powder feeding rate continues to increase, resulting in a decrease in the hardness of the cladding layer. With the gradual increase of powder feeding rate, the self-corrosion potential of the cladding layer moves positively and the self-corrosion current density decreases significantly. When the powder feeding rate reaches 10 g/min, the cladding layer shows the best corrosion resistance.

Disclosure Statement

No potential conflict of interest was reported by the authors.

References

1. Ampaw EK, Arthur EK, Badmos AY, Obayemi JD, Adewoye OO, Adetunji AR, et al. Sliding wear characteristics of pack cyanided ductile iron. J Mater Eng Perform. 2019;28:7227-7240. https://doi.org/10.1007/s11665-019-04471-8
2. Liu C, Du Y, Wang X, Zheng Q, Zhu X, Zhang D, et al. Comparison of the tribological behavior of quench-tempered ductile iron and austempered ductile iron with similar hardness. Wear. 2023;520:204668. https://doi.org/10.1016/j.wear.2023.204668
3. Wang B, Barber GC, Tao C, Sun X, Ran X. Characteristics of tempering response of austempered ductile iron. J Mater Res Technol. 2018;7(2):198-202. https://doi.org/10.1016/j.jmrt.2017.08.011
4. Larumbe LH, Delgado EH, Alvarez-Vera M, Villanueva PP. Forming process using austempered ductile iron (ADI) in an automotive Pitman arm. Int J Adv Manuf Tech. 2017;91(1):569-575. https://doi.org/10.1007/s00170-016-9771-1
5. Jhaveri K, Lewis GM, Sullivan JL, Keoleian GA. Life cycle assessment of thin-wall ductile cast iron for automotive lightweighting applications. Sustain Mater Technol. 2018;15:1-8. https://doi.org/10.1016/j.susmat.2018.01.002
6. Laine J, Leppänen A, Jalava K, Vaara J, Frondelius T, Orkas J. Ductile iron optimization approach for mechanically and thermally loaded components. Int J Metalcast. 2021;15:962-968. http://dx.doi.org/10.1007/s40962-020-00529-9
7. Tang YJ, Zuo XB, Yin GJ, He SL, Ayinde O. Influence of slag on leaching behavior of cement mortar lined in ductile iron pipe under a flowing solution. Mater Des. 2017;114:612-622. https://doi.org/10.1016/j.matdes.2016.11.096
8. Sun W, Yao B, Chen B, He Y, Cao X, Zhou T, et al. Noncontact surface roughness estimation using 2D complex wavelet enhanced ResNet for intelligent evaluation of milled metal surface quality. Appl Sci. 2018;8(3):381. https://doi.org/10.3390/app8030381
9. Wieczorek AN, Wójcicki M, Drwięga A, Tuszyński W, Nuckowski PM, Nędza J. Abrasive wear of mining chain drums made of austempered ductile iron in different operating modes. Mater. 2022;15(8):2709. https://doi.org/10.3390/ma15082709
10. Lukhi M, Kuna M, Hütter G. Numerical investigation of low cycle fatigue mechanism in nodular cast iron. Int J Fatigue. 2018;113:290-298. https://doi.org/10.1016/j.ijfatigue.2018.04.019
11. Sekiguchi S, Satou N, Shibata F. Mechanical properties of spheroidal graphite cast iron and stainless steel welded joints by electron beam welding. Strength Fract Comp. 2014;8(4):231-239. https://doi.org/10.3233/SFC-150172
12. Lei Y, Meng W, Ma Q, Yin X, Xie H, Hu L. Surface Alloying Characteristics of Inconel 625 Coatings Deposited on Ductile Cast Iron by Plasma Wire-Arc Welding. J Mater Eng Perform. 2023;1-4. https://doi.org/10.1007/s11665-023-08638-2
13. Mphela C, Phasha M, Moema J, van der Merwe J. Filler materials used to weld ductile cast iron–A review. MATEC web conf. 2022;370:04004. EDP Sciences. https://doi.org/10.1051/matecconf/202237004004
14. Bonabi SF, Ashrafizadeh F, Sanati A, Nahvi SM. Structure and corrosion behavior of arc-sprayed Zn-Al coatings on ductile iron substrate. J Therm Spray Tech. 2018 Feb;27:524-37. https://doi.org/10.1007/s11666-018-0694-2
15. Li Y, Dong S, Yan S, Li E, Liu X, He P, et al. Deep pit repairing of nodular cast iron by laser cladding NiCu/Fe-36Ni low-expansion composite alloy. Mater Charact. 2019;151:273-279. https://doi.org/10.1016/j.matchar.2019.03.021
16. Li Y, Dong S, He P, Yan S, Li E, Liu X, et al. Microstructure characteristics and mechanical properties of new-type FeNiCr laser cladding alloy coating on nodular cast iron. J Mater Process Technol. 2019;269:163-171. https://doi.org/10.1016/j.jmatprotec.2019.02.010
17. Liu Y, Yang Y, Chen C. A unique microstructure and its formation mechanism induced by laser cladding of Ti6Al4V alloy produced by

© Reseapro Journals 2024
https://doi.org/10.61577/jcti.2024.1000012

laser powder bed fusion. J Alloys Compd. 2024;996:174865. https://doi.org/10.1016/j.jallcom.2024.174865
18. Sun S, Wang J, Xu J, Cheng X, Jing C, Chen Z, et al. Preparing WC-Ni coatings with laser cladding technology: A review. Mater Today Commun. 2023;106939. https://doi.org/10.1016/j.mtcomm.2023.106939
19. Zhang H, Liu Y, Bai X, Zhao W, Zhang P, Rao WF. Laser cladding highly corrosion-resistant nano/submicron ultrafine-grained Fe-based composite layers. Surf Coat Technol. 2021;424:127636. https://doi.org/10.1016/j.surfcoat.2021.127636
20. Zhang H, Zou Y, Zou Z, Shi C. Effects of chromium addition on microstructure and properties of TiC–VC reinforced Fe-based laser cladding coatings. J Alloys Compd. 2014;614:107-112. https://doi.org/10.1016/j.jallcom.2014.06.073
21. Zhang H, Chong K, Xiao G, Sun Z, Zhao W. TIG cladding in-situ nano vanadium carbide reinforced Fe-based ultra-fine grain layers under water cooling condition. Surf Coat Tech. 2018;352:222-230. https://doi.org/10.1016/j.surfcoat.2018.08.032
22. Chang W, Xiao G, Zhang H, Chen H, Yi M, Zhang J, et al. Microstructure and properties of graphene reinforced co-based composite coating by laser cladding. Surf Coat Technol. 2023;453:129139. https://doi.org/10.1016/j.surfcoat.2022.129139
23. Tan Q, Liu K, Li J, Geng S, Sun L, Skuratov V. A review on cracking mechanism and suppression strategy of nickel-based superalloys during laser cladding. J Alloys Compd. 2024;175164. https://doi.org/10.1016/j.jallcom.2024.175164
24. Zhu L, Xue P, Lan Q, Meng G, Ren Y, Yang Z, et al. Recent research and development status of laser cladding: A review. Opt Laser Technol. 2021;138:106915. https://doi.org/10.1016/j.optlastec.2021.106915
25. Wang R, Ouyang C, Li Q, Bai Q, Zhao C, Liu Y. Study of the microstructure and corrosion properties of a Ni-based alloy coating deposited onto the surface of ductile cast iron using high-speed laser cladding. Mater. 2022;15(5):1643. https://doi.org/10.3390/ma15051643
26. Wei R, Mao M, Liang J, Zhao C, Ouyang C, Bai Q. Repair feasibility and performance enhancement analysis of Fe-based alloy coating on ductile iron surface by high-speed laser cladding. Mater Today Commun. 2024;39:108638. https://doi.org/10.1016/j.mtcomm.2024.108638
27. Yang P, Song Y, Wang J, Hu F, Xie L. Semiconductor laser cladding of an Fe-based alloy on nodular cast iron. Weld World. 2021;65(5):785-792. https://doi.org/10.1007/s40194-021-01078-3
28. Shu L, Zhang C, Li P, Cang X. Effects of Different Powder Feeding Rates on Microstructure and Mechanical Properties of IN718 Cladding Coating. Journal of Materials Engineering and Performance. 2023;1-10. https://doi.org/10.1007/s11665-023-08621-x

© Reseapro Journals 2024
https://doi.org/10.61577/jcti.2024.1000012